

# Performance Evaluation of a Triangular-Finned Absorber Plate Solar Air Heater: A Theoretical and Experimental Study

Pushkar Singh<sup>1</sup>, Vinod Singh Yadav<sup>1</sup>, T Sudhakar<sup>1</sup>, Vaibhav Trivedi<sup>2</sup>,  
Vineet Singh<sup>2,\*</sup>

<sup>1</sup>Department of Mechanical Engineering, National Institute of Technology Uttarakhand, Srinagar,  
Pauri (Garhwal) 246174, Uttarakhand, India

<sup>2</sup>Department of Mechanical Engineering, School of Engineering and Technology, IFTM  
University, Moradabad, 244102, India

\*Author to whom correspondence should be addressed:

E-mail: vineet.singh@iftmuniversity.ac.in

(Received May 05, 2025; Revised August 12, 2025; Accepted September 04, 2025)

**Abstract:** The thermo-fluid performance of triangular finned absorber plate solar air heater (SAH) can be enhanced using numerous favorable and effective techniques. These methods improve the heat transfer coefficient (HTC) at interface of the circulating fluid (fresh ambient air) and solar air collector or absorber plate. Fixing small, novel fins to the absorber plate enhances thermal performance by improving the airflow path of ambient air across the plate. Novel absorber plate design, optimized flow sections, and added turbulence via fins, ribs, or baffles enhance the performance of SAH. This investigation examines theoretical and experimental analyses on enhancing the thermo-fluid performance of a SAH by attaching a novel triangular-shaped fin design to the absorber plate and arranging the fins in an innovative pattern. The assessment of this work focused on enhancing heat transfer while minimizing the pressure drop. The system operates on solar thermal technology, utilizing heat derived from solar energy. Solar irradiance encroaches on glazing, where it's partly absorbed by the black absorber plate and fins, and partly heats the air circulating between the transparent glazing and triangular finned absorber plate. Based on this setup, various performance-related equations were derived under several simplifying assumptions. The analysis was conducted at mass flow rates (MFR) ranging from 0.010 to 0.015 kg/s, with results showing an enhanced thermo-fluid performance of the rectangular duct SAH. The maximum inlet air temperature reached 59 °C at the lowest mass flow rate MFR of 0.010 kg/s across whole day, with the peak temperature occurring at a solar flux of 846 W/m<sup>2</sup>. The heat transfer coefficient increased from 3.20 W/m<sup>2</sup>K to 13.84 W/m<sup>2</sup>K with variability in MFR and solar flux during the whole day. The assessment of this study reveals a 6.25% variation between theoretical and experimental pressure drop at the lowest MFR of 0.010 kg/s.

**Keywords:** Collector; Heat transfer enhancement; Solar air heater; Thermal performance; Triangular finned absorber plate

## 1. Introduction

The present global scenario on conventional sources of energy and oil resources may be wiped out after few years due to the scarcity of traditional energy sources and oil reserves. Since the availability and reliability of petroleum is uncertain in future. This is the crucial time that we must focus on alternate energy resources to fulfil our future demands of petroleum and energy<sup>1</sup>). Because of global warming now days the temperature of the environment is rising as time passes. This temperature rise is because of the greenhouse gas emissions in our atmosphere<sup>2</sup>). The concentration of greenhouse gases in our environment is

continuously increasing day by day<sup>3</sup>). This is because of the main source of greenhouse gasses is emissions from industries and automobiles<sup>4</sup>). Global warming is the main cause of the melting of mountain glaciers; causing to rising of sea levels. If this rise in sea level continues, some low laying area countries in the world<sup>5</sup>).

Our unstoppable and continuous use of huge conventional energy resources without keeping in mind sustainable development is the main cause of environmental problems and future petroleum problems<sup>6</sup>). So, the need for renewable energy sources and alternate energy resources came into focus; for a clean and pollution free

environment which leads to need of research on biofuels and renewable energy sources for zero emissions<sup>7-9</sup>).

Solar thermal technology uses an absorbing material to heat air with solar energy<sup>10</sup>). This technology is used to heat or conditioned the fresh air for the single or multistoried buildings, crops drying applications, offices, and preparing greenhouses. Solar air heaters (SAHs) are used as a supplement of conventional air heating systems. At the absorber surface of black-painted absorber plates (AP), SAHs convert the sun's irradiance or solar flux into thermal energy (heat). This heat is subsequently transferred to a flowing fluid (air) passing through finned solar air collector<sup>11</sup>).

SAHs have been widely used as a cost-efficient and eco-friendly method for space heating, heating buildings, drying crops, and other applications that require the use of hot air<sup>12</sup>). Over the years, research has been conducted by the researcher<sup>13-17</sup>) to boost the thermo-hydraulic performance (THP) of the solar air heating system by optimizing various components of SAHs; such as the geometrical parameters of the absorber tray, extended surfaces, air ducts, glazing, insulation, spacing between the fins or tubes or ribs, and tilt angle. A series of studies<sup>18-22</sup>) were conducted to improve the THP of SAHs. These studies focused on the placement of arc-shaped ribs at various locations and aimed to established empirical relationship for friction factor (FF) and heat transfer (HT). As a result, correlations for HT and friction factor were established. The temperature profile in individual component of a SAH can be computed by applying heat energy balance equations. Numerous researchers<sup>23-27</sup>) have theoretically examined various collector designs and found that a collector length of 1 meter can yield satisfactory performance. Daily average thermal, exergy, and thermohydraulic efficiencies of 29.55%, 14.59%, and 7.24%, respectively, were achieved by the modification of flat plate SAH introducing rotating spiral-shaped baffles on absorber plate<sup>28</sup>). A numerical investigation is conducted to examine how a non-flat AP influences the performance of a SAH. The non-flat geometry promotes airflow turbulence, thereby enhancing average thermal efficiency from 28.8 to 54.7 %. Throughout the day, the non-flat AP demonstrated up to a 141.5% enhancement in the Nu relative to the flat plate configuration<sup>29</sup>). The study shows that placing polygonal-shaped ribs at the duct center yields the highest improvement in heat transfer performance<sup>30</sup>). Investigation on THP of SAH using quarter circle roughness ribs reveals the increased value Nu and the decreased value of average FF. The introduction of artificial roughness on the AP results in a substantial enhancement of the Nu relative to that of a smooth surface, due to improved turbulent heat transfer. At a Reynolds number of 16,000 and a p/e ratio of 6.67, the quarter-circle roughened duct achieved a 2.42-fold increase in the Nu relative to the smooth duct<sup>31</sup>). Hence

introducing roughness or ribs on collector improves the thermal performance of SAH. Artificial roughness effectively enhances heat transfer in solar air heaters compared to smooth surfaces but increases flow friction and pumping power. Both the Nusselt number and friction factor are influenced by the Reynolds number; as Re increases, turbulence intensifies, boosting Nu, while the thinning viscous sublayer reduces f. With the implementation of discrete double arc ribs, the friction factor exhibited an inverse relationship with the Re, increasing as Re decreased<sup>32</sup>).

### 1.1. Research gaps

Solar air heaters (SAHs) typically suffer from limited efficiency due to challenges in heat transfer. A widely used approach to enhance performance involves introducing roughness elements to the absorber plate. However, stationary roughness elements can create localized heating and thermal disturbance regions, which impede effective convective heat transfer. Use of ribs or fins makes the artificial roughness along the cross-section of duct, which leads to more turbulence of air in flow channel and increase in heat transfer coefficient<sup>33-35</sup>). The impact of MFR of working fluid on the outlet temperature of heated air, HTC and pressure drop has been evaluated for the improvement in THP of SAH<sup>36</sup>). Despite significant advancements in SAH technology, several research gaps remain. Most studies focus on performance under optimal solar conditions, with limited investigation into SAH performance during fluctuating or low solar intensity. The integration of smart thermal energy storage systems is often inefficient, and innovative fin or absorber geometries such as dynamic or biomimetic designs are underexplored. Hybrid configurations with other renewable systems remain unoptimized, and the use of heat storage phase change materials (PCMs), advanced materials prone to high emissivity, and intelligent and smart control systems, such as artificial intelligence and machine learning, is still limited. Additionally, life-cycle cost and environmental impact assessments are often underexplored. Number of theoretical and experimental studies<sup>37-48</sup>) have been carried out to investigate the thermo-fluid performance of SAH, but very few attempts has been performed on triangular finned absorber plate made of aluminium material and arrangements of fins pattern. Most research on SAHs focuses on ideal conditions, with few studies examining their performance under low solar intensity.

### 1.2. Novelty and objectives of the present work

Investigations on triangular finned absorber plate SAH have been performed in very less numbers due to the convoluted flow dynamics and the limitations in welding process, for welding of fins onto aluminum metal absorber plate. To address these limitations, this study explores a

modified design of a rectangular duct SAH incorporating a novel design absorber plate having triangular fins and their unique cross (X) arrangement. This study aims to evaluate the thermo-fluid performance of a novel rectangular duct SAH incorporating a uniquely designed triangular finned absorber plate. The cross (X) arrangement of fins on the absorber plate in a solar air heater is a smart thermal design strategy aimed at improving heat transfer and enhancing air turbulence for better overall efficiency. The X-shaped fin configuration increases the surface area available for heat exchange between the absorber plate and the air. More contact area allows more heat to be transferred from the plate to the moving air. The intersecting fin design disturbs the airflow, breaking up smooth (laminar) flow and creating turbulent eddies. Turbulence leads to better mixing of air layers, minimizing the thermal boundary layer and increasing the rate of convective heat transfer. The primary focus of this study is to enhance heat transfer while simultaneously minimizing pressure drops along the duct of the SAH. Both theoretical mathematical modeling and experimental analysis have been conducted to assess the system's overall thermo-fluid performance.

## 2. Theoretical investigation of a triangular finned absorber plate solar air heater

### 2.1. Model equations for new designed solar air heater

Model equations for the triangular finned type absorber plate SAH has been formulated under following assumptions such as:

- Analysis is performed when SAH system is in steady state conditions with steady airflow.
- The temperature of air is supposed to be uniform through the flow cross-section.
- Air is deemed to be an ideal fluid i.e.; specific heats of air remain unchanged.
- Heat conduction is regarded as being minimal.
- Temperature variation in both the inlet air and absorber plate are restricted to the flow direction.
- The convective HTC outside remains constant along the length of SAH.
- The heat flow through a cover is considered to be one dimensional.

Theoretical analysis for the novel designed rectangular duct triangular finned SAH has been conducted based on the above assumptions. Thermal network for the rectangular duct triangular finned SAH shows the various mode of HT between absorber plate and glazing, AP and flowing air, and cover plate and flowing air. Configuration diagram of SAH, SAC and thermal network is presented

in Figure 1.

Thermal energy balance equation for the thermal circuit represented in Figure 1 has been modeled as:

Thermal energy conservation equation for glass cover plate:

$$U_{itAC}(T_C - T_{air}) = h_{cfAC}(T_f - T_C) + h_{repAC}(T_P - T_C) \quad (1)$$

Where, mean fluid temperature  $(T_f) = (T_{fi} + T_{fo})/2$

Energy balance equation for collector or absorber plate

$$I\alpha_{AP} = U_{blAP}(T_P - T_{air}) + h_{pfAP}(T_P - T_f) + h_{repAP}(T_P - T_C) \quad (2)$$

Where,  $h_{rep}$  is the relative HTC between toughened glazing and AP, and may be evaluated either by using Eqn. (3) or (4), both equation gives the same value.

$$h_{rep} = \frac{\sigma(T_P^2 + T_C^2)(T_P + T_C)}{\left(\frac{1}{\epsilon_P}\right) + \left(\frac{1}{\epsilon_C}\right) - 1} \quad (3)$$

Absorber plate temperature ( $T_P$ ) is calculated as follows:

$$T_P = \frac{(T_{P1} + T_{P2} + T_{P3} + T_{P4} + T_{P5} + T_{P6} + T_{P7} + T_{P8})}{8}$$

Where,  $T_{P1}$ ,  $T_{P2}$ ,  $T_{P3}$ ,  $T_{P4}$ ,  $T_{P5}$ ,  $T_{P6}$ ,  $T_{P7}$ ,  $T_{P8}$  are the temperature measured at various locations of absorber plate.

If radiation ( $\dot{Q}_u$ ) between any two arbitrary surfaces are given then HTC may also be evaluated by Eqn. (4)

$$\dot{Q}_u = h_{rep}A_P(T_P - T_C) \text{ i.e. } h_{rep} = \left(\frac{\dot{Q}_u/A_P}{(T_P - T_C)}\right) \quad (4)$$

The correlation for determining the thermal radiation HTC ( $h_{cs}$ ) between the sky and glass cover plate (glazing) is as follows in Eqn. (5):

$$h_{cs} = \frac{\sigma \epsilon_c(T_C + T_s)(T_C^2 + T_s^2)(T_C - T_s)}{(T_C - T_a)} \quad (5)$$

Temperature of sky ( $T_s$ ) is measured by the correlation shown in Eqn. (6)<sup>49,50</sup>:

$$T_s = 0.0552 T_{air}^{1.5} \quad (6)$$

Theoretically it is difficult to calculate the average ambient temperature of SAC or absorber plate, since it is the function of solar insolation on absorber plate, design of collector and inlet fluid conditions. Therefore, theoretical efficiency of collector is measured by Eqn. (7).

$$\eta_{collector} = \frac{\dot{Q}_u}{\dot{Q}_C} = \frac{A_P F_R [(\tau\alpha)I - U(T_{fi} - T_{air})]}{I A_P} \quad (7)$$

Where,  $F_R$  is the heat removal factor of solar air collector.

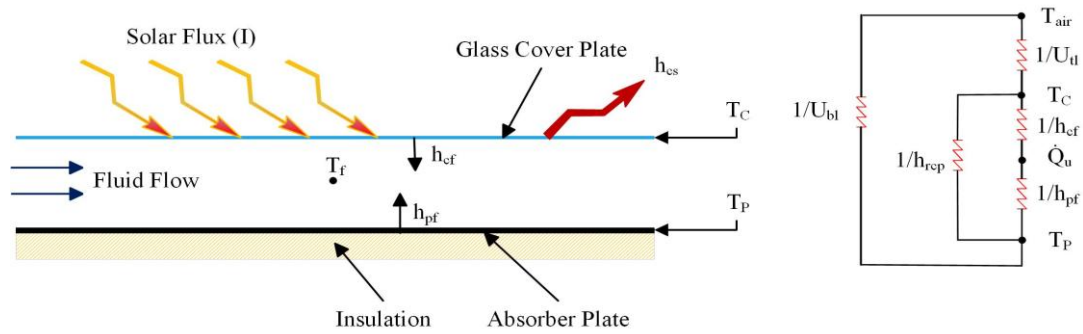


Fig. 1: Configuration diagram of a triangular-fin solar air collector and its thermal network

## 2.2. Thermal analysis

### 2.2.1. Heat conversion (thermal) efficiency of triangular finned solar air heaters

The thermal efficiency ( $\eta_{th}$ ) of SAH or SAC may be expressed as “the ratio of useful solar energy to the overall amount of incident solar flux, and calculated by using the given equation”<sup>51-55</sup>.

$$\eta_{th} = \frac{\dot{Q}_u}{\dot{Q}_c} = \frac{\dot{m}_f C_{pf} (T_{fo} - T_{fi})}{IA_p} \quad (8)$$

The term  $\dot{Q}_u$  is the useful heat gain or energy gain and  $\dot{Q}_c$  is direct incoming solar radiation in Eqn. (8). These terms are further calculated by using following formulas:

$$\dot{Q}_u = \dot{m}_f C_{pf} \Delta T_f = \dot{m}_f C_{pf} (T_{fo} - T_{fi}) \text{ and } \dot{Q}_c = IA_p \quad (9)$$

### 2.2.2. Evaluation of heat transfer coefficient and Nusselt number

The correlation developed by McAdams<sup>56</sup> is utilized to determine the coefficient of heat convection ( $h_w$ ) from ambient wind over the outer surface (i.e. wind flowing on top surface of glazing or transparent glass cover) having outside wind velocity ( $V_w$ ):

$$h_w = 5.7 + 3.8 V_w, \text{ where, } (0 \leq V_w \leq 5 \text{ m/s}). \quad (10)$$

### 2.2.3. Mass flow rate

MFR of flowing fluid (air) across the flow section depends on air velocity and is evaluated as follows:

$$\dot{m}_f = \rho_{air} A_f V_{air} \quad (11)$$

Following correlations developed by Kays<sup>57</sup> has been used to evaluate the convective HTC for the turbulent ( $Re \geq 2300$ ) forced convection flow between the flowing fluid and toughened glass cover plate, and between the SAC and the bottom plate.

$$h = \frac{Nu K}{D_h} \quad (12)$$

Nusselt number is calculated by Dittus-Boelter's Correlation<sup>58</sup> given in eqn. (13)

$$Nu = \frac{h D_h}{K} = 0.023 Re^{0.8} Pr^{0.4}, \text{ when } 160 \geq Pr \geq 0.7 \quad (13)$$

Where, hydraulic diameter ( $D_h$ ) =  $\frac{4 (\text{Wetted Area})}{\text{Wetted perimeter}}$

$$\frac{4A_{wet}}{P_{wet}} = \frac{4(w \times h)}{2(w+h)}$$

Hydraulic diameter is a characteristic length used to analyze flow and heat transfer in non-circular ducts for analyzing flow characteristics like pressure drop and heat transfer. Hydraulic diameter is crucial for calculating Reynolds and Nusselt numbers in non-circular ducts, enabling accurate modelling of airflow and heat transfer in solar air heaters. It also aids in determining pressure drop and pumping power using the Darcy-Weisbach friction factor, which relies on Reynolds number based on hydraulic diameter.

## 2.3. Hydraulic performance analysis

### 2.3.1. Reynold number

Reynolds number is calculated by using following equation:

$$Re = \frac{\rho V D_h}{\mu_{air}} = \frac{\dot{m}_f D_h}{A_f \mu_{air}} \quad (14)$$

### 2.3.2. Friction factor

Friction factor is calculated by Blasius Correlation<sup>58</sup> given in Eqn. (15).

$$f = 0.0791 (Re)^{-0.25}, \text{ when, } Re \geq 4000 \quad (15)$$

### 2.3.3. Pressure drop

Pressure drop along the testing zone was calculated by Eqn. (16) with the help of friction factor obtained by Eqn. (15)

$$\Delta P = \frac{\rho_{air} L_t V_{air}^2 f}{2 D_h} \quad (16)$$

### 3. Experimental setup design and fabrication

Figure 2 present the pictorial view of a novel designed experimental setup of SAH. A rectangular duct SAH was designed and fabricated consisting of a SAC i.e. absorber plate; which is made of aluminium having triangular fins fixed on it. Triangular fins are attached with the absorber plate by the tungsten inert gas (TIG) welding process due to limitation of welding processes for aluminium material. Tungsten inert gas welding is also named as gas tungsten arc welding. Figure 2 presents the pictorial view of rectangular duct triangular finned SAH. The experimental setup features a newly designed absorber plate with triangular fins, arranged in cross (X) pattern to create more and more turbulence and enhance the HT rate. A rectangular wooden box has been designed according to the dimension of SAC to support it. The solar air collector has the rectangular geometry and measuring size of 1.22 m x 0.455 m, made of aluminium (Al) sheet of thickness 2 mm. Box is insulated from both inner and outer side with styrofoam and glass wool insulation of thickness 6 cm at inside and hitlon of thickness 3 cm at outside to prevent the heat loss. A toughened glass cover plate of thickness of 5 cm is attached on top of the wooden box to maintain the pressurized fluid flow and also prevent the up flow of air from the rectangular duct flow channel. Two ducts made of GI sheet of 18 gage is attached at the outlet and inlet of rectangular box. The designed of duct of SAH is according to ASHRAE standard. The length of inlet and outlet duct has been considered as  $L \geq 5\sqrt{(w \times h)}$  and  $L \geq 2.5\sqrt{(w \times h)}$  respectively as stated by ASHRAE standard<sup>59)</sup>, where 'w' and 'h' are the width and height of flow cross section of duct. Setup is supported by a steel frame attached with wheels so as to easy handling and transportation from one place to another place. SAH is installed on frame having inclination of 29° and has south direction such that the solar flux falls normal to the absorber plate. Setup consist of an instruments box for the safe and easy handling of instruments collecting of more accurate data during data recording. Thermocouples are

attached at various locations to record the temperature at various locations on absorber plate. An air blower is attached at the inlet duct to ensure the continuous and uniform supply of air to the SAH.

Air blower has six variable speed and is connected to the inlet duct by an air pipe. Digital micro-manometer is attached at the entry and exit of test zone to record the pressure drop along the testing zone. Pressure drop can also be measured by using mercury filled U-tube manometer.

#### 3.1. Design parameters for solar air heater

Designed parameters for SAC and SAH are represented in Table 1.

Experimental setup for SAH is designed and fabricated properly and based on solar-thermal technology, where heat is carried out in solar air dryer from solar air collector through a working fluid (air).

#### 3.2. Thermo-physical properties of working fluid

Thermal and physical properties of air are presented in Table 2.

#### 3.3. Experimental procedure and methodology

Based on previous research, a SAH operated on solar energy has to be theoretically designed. The theoretical design consists of the size of solar collector or absorber plate, absorber tray, ducts, design of fins, number of fins, arrangements of fins, the number of solar collectors, and the capacity and power of the blower or fans. After determining theoretically, the size of each component of the SAH, the triangular shaped finned SAH has to be installed at research location. The performance analysis of the SAH has to be calculated theoretically and experimentally and compared both results. The methodology for the design and analysis of SAH is presented in Figure 3. SAH works on solar-thermal technology. SAH is a sustainable and renewable energy heating technology. Solar flux direct incident on normal to the surface of glass cover plate and then heat coming

**Table 1:** Designed parameters for absorber plate/solar air heater

Sr. No.	Parameters	Value/Range/Material
	Dimension	1.22 m x 0.455 m
	Type of Collector/Absorber Plate	Triangular Finned and Black Painted
	Types of Glazing/Cover Plate	Single Toughened Glass
	Working Fluid	Air
	Flow Area of Duct	0.0192 m <sup>2</sup>
	Thickness of Insulation (t <sub>b</sub> , t <sub>e</sub> )	0.06 m, 0.03 m
	Material of Collector	Aluminium
	Material of Fins	Aluminium
	Number of Fins	80

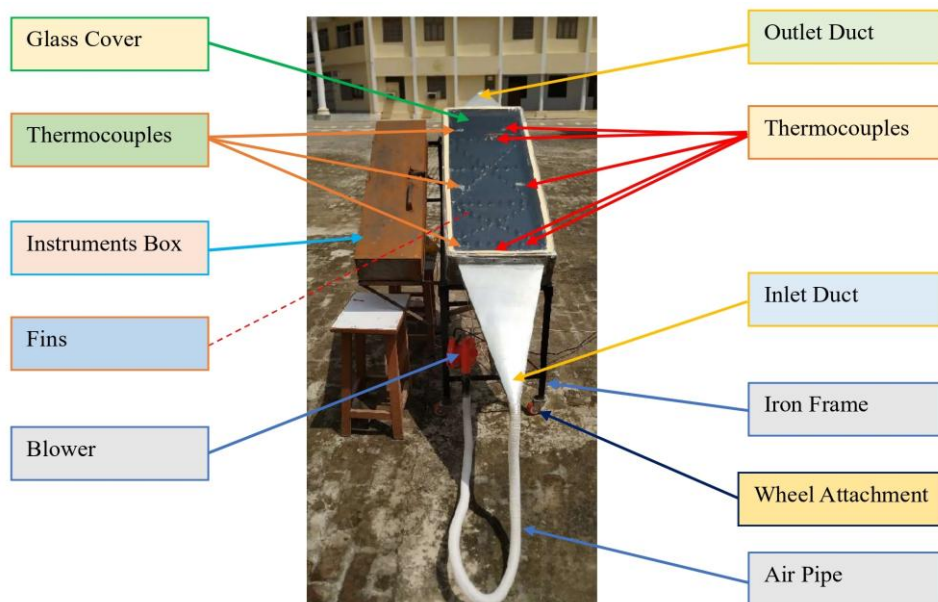


Fig. 2: Visual representation of experimental setup

Table 2: Thermo-physical characteristics of circulating fluid (air).<sup>58,60</sup>

Sr. No.	Properties of air/Parameters	Value/Range
	Working Fluid	Ambient Air
	Dynamic Viscosity of Air ( $\mu_{air}$ )	$1.846 \times 10^{-5}$ Ns/m <sup>2</sup>
	Specific Heat of Air ( $C_p$ )	1.007 kJ/kg/K
	Density of Air ( $\rho_{air}$ )	1.1614 kg/m <sup>3</sup>
	Prandtl number (Pr)	0.7

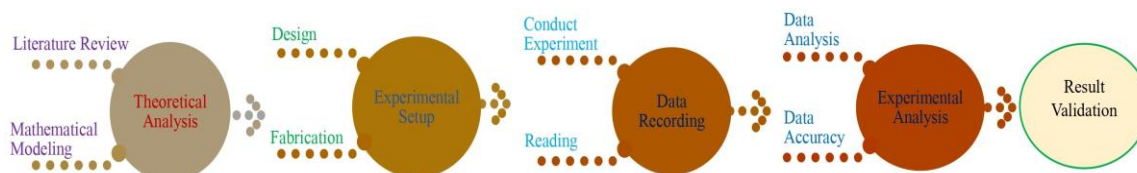


Fig. 3: Experimental procedure and methodology

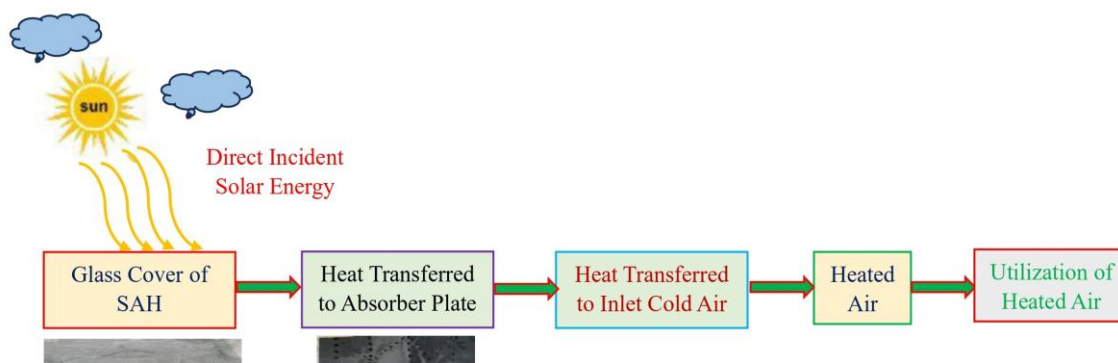


Fig. 4: Solar air heating and heat flow through solar air heater

from solar energy is transferred from cover plate to the absorber plate. This heat from absorber plate is transferred to the cold air entering at the inlet of test section. This

heated air is used for various heating applications. Heat flow phenomena are shown in Figure 4. Experiment was conducted at a location having latitude 28° 46' 22.80" N

**Table 3:** Error in measuring instruments

S. No.	Parameter	Error (%)
1	k-type thermocouples	2
2	Pyranometer (Solar Flux)	1.8
3	Digital Anemometer	2.5
4	Micro-Manometer	1.8%

and longitude 78° 41' 19.66" E with variation in MFR from  $m1=0.010$  kg/s to  $m6=0.015$  kg/s. An experimental study has been executed in the month of September 2023 (for rainy season). Prior to initiating the air flow in the duct, all thermocouples were calibrated to ensure accurate room temperature readings, and a digital manometer is used to detect any potential leakage. The tests are performed under the steady-state conditions to record precise data on HT and fluid flow friction. Steady-state conditions are considered to be achieved, when the temperatures recorded by each thermocouple remain constant for a period of 5-10 minutes. As the study state is achieved test is performed on experimental setup for data recording purpose. All data were recorded throughout the day to account for the variation in solar flux with time.

### 3.4. Measuring instruments

Various measuring instruments such as digital thermo-anemometer, solar power meter, micro-manometer etc. has been used to measure the velocity, solar flux and pressure drop. K-type thermocouple with digital temperature scanner was used at eight positions of absorber plate to find the mean temperature of AP. A pair of thermocouples was employed at the entry and exit section to find the outlet and inlet temperature of flowing fluid and one thermocouple was utilized to determine the glass cover temperature. Two K-type thermocouples were used, one at the fin's base and other at the tip of the fin to record the temperature variation along the height of the fin. A blower of six adjustable speed was used to maintain the uniform velocity of circulating air along the test section of SAH. Solar power meter was used to find the variation in solar flux or solar intensity along the time of the day. The error in various components is represented by Table 3.

## 4. Results and discussions

The theoretical results computed from the theoretical modeled equation and the experimental result obtained from experimental setup has been discussed in this section. Theoretical result consists of variation of Re, Nu and HTC; with variation of MFR from  $m1=0.010$  to  $m6=0.015$  kg/s, respectively. Reynold's number is varying from  $Re=14851$  to  $Re=22342$  with increase in MFR. General trends of increase in Re with MFR can be seen in numerical study while using semi-circular transverse rib<sup>61</sup>). As the Re is increased, heat transfer coefficient increased from  $3.20$  W/m<sup>2</sup>K to  $13.84$  W/m<sup>2</sup>K

with the increased Nu from 10.38 to 14.40. The experimental results include the variation of circulating air temperature at outlet, inlet and solar flux, dependent on time of day<sup>62,63</sup>). Figure 9 shows the variation in irradiation level, ranging from  $318$  W/m<sup>2</sup> to  $846$  W/m<sup>2</sup>, throughout the day, from 09:00 AM to 05:00 PM and maximum solar flux was found around 12:00 PM to 01:00 PM.

### 4.1. Flow characteristics: heat transfer coefficient, Reynold's number and Nusselt number

As the MFR increased, both the fluid velocity and the Reynolds number were found to rise due to their interdependent relationship. At lower MFR, the Re was also found to be low. In this regime, the flow remained laminar, as the reduced mass flow rate resulted in lower velocities that were not enough to overcome the viscous forces. As a result, the flow remained steady and smooth with minimal turbulence<sup>64</sup>).

This work presents that Reynold's number is varying from  $Re=14851$  to  $Re=22342$  with the increase in MFR, shown in Figure 5, similar result presented in<sup>65-67</sup>). As the velocity increases the MFR increases, causes to increased Re. Nusselt number increases with the increase in MFR<sup>68</sup>). Another study shows that as the MFR increased, the Re increased significantly<sup>69</sup>). With the higher flow rate, the fluid velocity also rose, pushing the Re past the threshold where laminar flow transitioned into a turbulent regime. At this point, the fluid velocity became high enough for inertial forces to dominate over viscous forces, initiating turbulence<sup>70</sup>). Study has been found that at high mass flow rates, the Re reached its peak, and the flow became largely turbulent. The higher flow rate led to significantly increased velocities, which resulted in much higher Reynolds numbers. In this regime, the flow exhibited chaotic and irregular patterns, characterized by eddies, vortices, and turbulence<sup>71</sup>).

The findings of this work shows that the Nu increases as the Re increases<sup>72</sup>), while the friction factor (FF) decreases with an increase in Reynold's number<sup>73</sup>). This study examined the variation of the friction factor (f) and Nusselt number (Nu) as functions of the Reynolds number (Re) in a specific flow system. Figure 6 reveals the increase of Nu from 10.38 to 14.40, with the increase in MFR and Reynold's number. The presence of a turbulator markedly enhances the Nusselt number by influencing both thermal energy transfer and flow dynamics, with effects varying by design<sup>74</sup>). Figure 7 reveals the variation of HTC with MFR. As the MFR increases Reynolds number shows the increasing trends from  $3.20$  W/m<sup>2</sup>K to  $13.84$  W/m<sup>2</sup>K. A study found that increased Re and MFR enhance airflow turbulence, thereby improving convective heat transfer<sup>75</sup>).

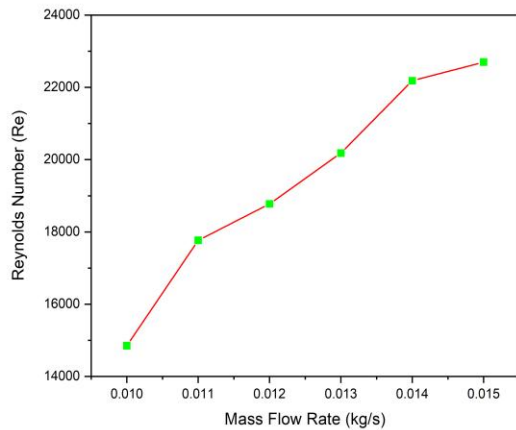


**Fig. 5:** Effect of mass flow rate on Reynolds number

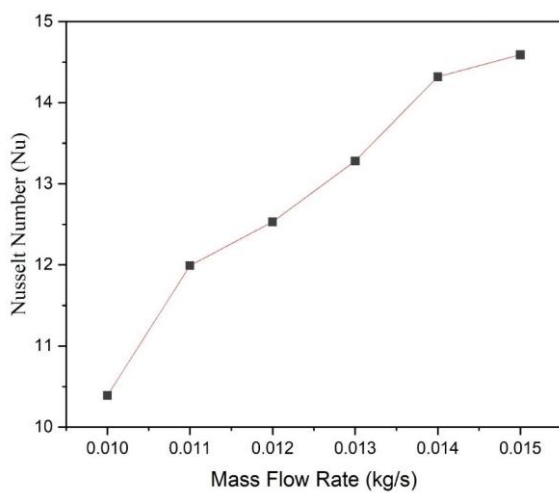


**Fig. 6:** Effect of mass flow rate on Nusselt number

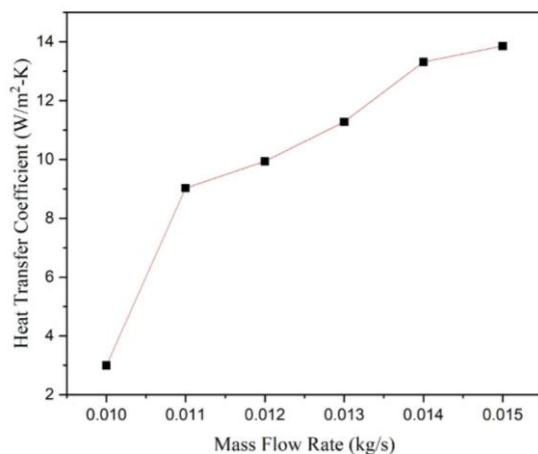


**Fig. 7:** Effect of mass flow rate on heat transfer coefficient

As the Re increased, the Nu also increased, which aligns with the principles of convective HT. The Nusselt number, representing the enhancement of HT due to fluid motion, typically rises in turbulent flow. In laminar flow,

HT is primarily or mainly due to the conductive mode of heat transfer, resulting in a lower value of Nu. As the Reynold's number increases, the fluid flow becomes more and more turbulent, improved mixing of fluid and enhances heat transfer, leading to a higher Nusselt number. The study has been found that both the Nusselt number and the HTC increased with an increase in Reynolds number<sup>76</sup>.

A study found that triangular rib roughness in triangular finned SAHs boosts the Nusselt number by 1.4 to 2.7 times in comparison with smooth ducts<sup>77</sup>.

#### 4.2. Variation solar flux, inlet and outlet temperature

Figure 8 shows that outlet temperature of air decreases as the MFR increased, faster the air flows through a system, the less time it will be in association with the collector. Maximum temperature of air was achieved to be 59 °C at lowest MFR of  $m_1=0.010$  kg/s and minimum outlet temperature of 57 °C at the highest MFR of  $m_6=0.015$  kg/s, around 12:00 PM. A higher MFR of air lowers the outlet temperature because it reduces the contact time between the SAC and the air<sup>78</sup>. Outlet temperature of air is highest at lower mass flow rate because less quantity of air is retaining for more time duration inside the solar air heater. This is likely caused by the reduced channel height, which decreases the cross-sectional area of the airflow and results in a higher HTC on the AP surface. Consequently, the outlet temperature of the finned AP increased as the air carried away more heat. Therefore, the findings suggest that reducing the airflow's cross-sectional area and increasing airspeed enhance the convective HT efficiency of the AP, causing a progressive enhancement in thermal efficiency of heat collector<sup>78,79</sup>. Figure 9 represent the time dependent behavior of solar flux. Variation of solar flux has been found from 436 W/m<sup>2</sup> to 318 W/m<sup>2</sup> along the time of the day starting from morning 09:00 AM to 05:00 PM respectively with a peak value of 846 W/m<sup>2</sup>. Figure 10 represent variation of outlet and inlet temperature of air from beginning to end of day; temperature of inlet air was increased from 30 °C to 47 °C at starting of day around 09:00 AM when the MFR was 0.010 kg/s. The temperature of inlet air was increased from 42 °C to 59 °C at lowest MFR 0.010 kg/s along with time of the day, and at a highest solar flux of 846 W/m<sup>2</sup> around 12:00 PM. Temperature of the inlet air was increased by 56.66 % to 40.47 % with changes in daylight. Solar flux is varying from 436 W/m<sup>2</sup> to 846 W/m<sup>2</sup>; throughout the day due to increase in solar flux or solar intensity<sup>80</sup>. Maximum solar flux was found in between 12:00 PM to 01:00 PM along the time of day.

#### 4.3. Variation of pressure drop with mass flow rate

This study reveals that pressure drops of flowing air along

the rectangular duct of the SAH increase with the increase in MFR and Reynold's number<sup>81</sup>). As MFR increases, air velocity rises, leading to more friction and a higher PD, since pressure drop is proportional to the square of velocity. At low MFR, the flow is typically laminar with lower friction. As flow rate increases, the flow becomes turbulent, causing more energy loss and a larger PD. This transition is indicated by an increasing Reynolds number. Figure 11 present the experimental pressure drop result obtained by the data recorded from digital micro-manometer. This study shows the increase in pressure drop from  $6 \text{ N/m}^2$  to  $18 \text{ N/m}^2$ ; with the escalation in MFR ranges from  $0.010 \text{ kg/s}$  to  $0.015 \text{ kg/s}$ , respectively. Peak pressure drop has been recorded at the higher MFR of  $0.015 \text{ kg/s}$ . Study aims to minimize the pressure drop (PD) along the duct of SAH; minimum pressure drop achieved at a minimal MFR of  $0.010 \text{ kg/s}$ . Pressure drops increases along the length of AP, due to the friction between AP and flowing air. Similar trends of increase of pressure drop were shown by a different study<sup>82</sup>).

#### 4.4. Comparison in pressure drop of theoretical and experimental result

Figure 12 shows the comparison between the theoretical pressure drop result obtained by theoretical analysis and experimental pressure drop result obtained by recording data from digital micro-manometer. There is variation in the result obtained from theoretical calculation and experimental analysis, this variation in both results found to be less at lower MFR of  $0.010 \text{ kg/s}$  and more at higher MFR, as shown in Figure 12. This work found minimum variation of  $6.25 \%$  in theoretical and experimental pressure drop at MFR of  $0.010 \text{ kg/s}$ ; while the maximum variation of theoretical and experimental result of  $30.55 \%$  at MFR of  $0.015$ . Variation in pressure drop obtained by theoretical and experimental result increases as the MFR increases, due to the presence of more and more fins. Researcher has investigated the similar trends in variation of pressure drop (PD) with MFR. Fins are used to enhance convective HT; however, because of presence of multiple obstacles or fins attached with absorber plate, there is a slight chance that the PD may increase<sup>83</sup>). Also, with the increases in MFR, pressure drops increases due to the higher velocity of airflow<sup>84</sup>).

#### 4.5. Effect of mass flow rate and Reynold's number on the friction factor

The results of this study indicate that the friction factor (FF) was observed to be decrease as the Re increased. As the Re increases, both the FF and Stanton number decrease, primarily because inertial forces surpass viscous forces, reducing flow resistance<sup>85</sup>). Figure 13 reveals that the FF decreases from  $0.0065$  to  $0.0058$  as the MFR increases ranges from  $0.010$  to  $0.015 \text{ kg/s}$ . Higher values of friction factor is obtained at lower MFR of  $0.010 \text{ kg/s}$

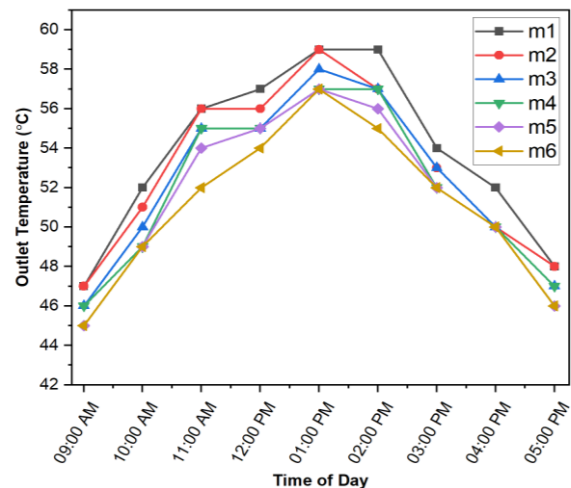


Fig. 8: Outlet temperature variation over the day at different mass flow rates

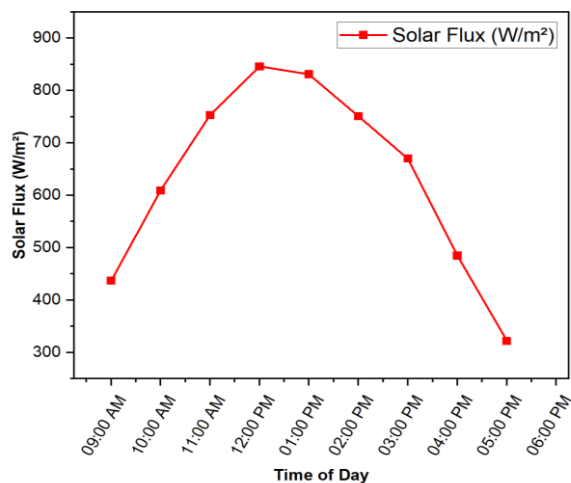
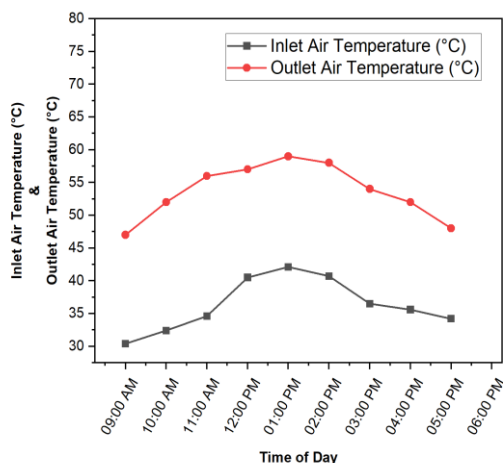


Fig. 9: Time-dependent behavior of solar flux

and lowest value of friction factor was found at highest MFR of  $0.015 \text{ kg/s}$ . At lower Reynold's numbers, the flow is predominantly laminar, which results in a higher value of FF. As the Re increases, the flow converted from transitions to turbulence, where inertial forces dominate over viscous forces, leading to a reduction in the friction factor. This behavior is characteristic of flow in pipes or ducts, where higher Reynolds numbers decrease the frictional resistance due to enhanced mixing and a thinner laminar sublayer. Similar results were obtained by many researchers from the study of finned type SAH<sup>86-88</sup>). Less viscous force at high MFR reduces the frictional resistance offered, leads to lower friction factor<sup>89</sup>).

## 5. Conclusions

The theoretical results derived from the modeled equations and the experimental results obtained from the experimental setup have been analyzed and discussed in result section and it has been concluded as following:



**Fig. 10:** Variation of inlet and outlet air temperature over the time of day.

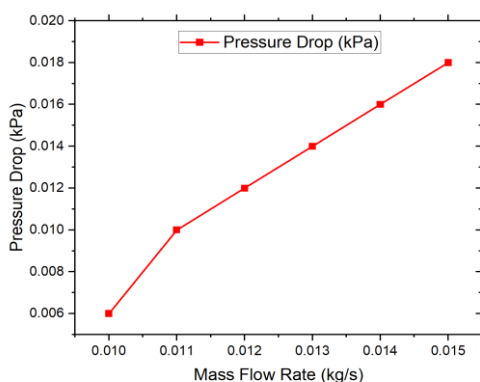


**Fig. 11:** Pressure drop variation with mass flow rate

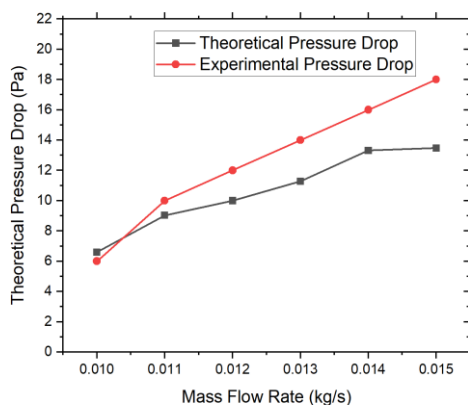


**Fig. 12:** Comparison in pressure drop of theoretical and experimental result

The theoretical results show that as the MFR increases from 0.010 kg/s to 0.015 kg/s, the Reynolds number rises from 14851 to 22342. Consequently, the heat transfer coefficient increases from 3.20 W/m<sup>2</sup>K to 13.84 W/m<sup>2</sup>K, and the Nusselt number increases from 10.38 to 14.40. The Nu is found to increase with both the Re and MFR.

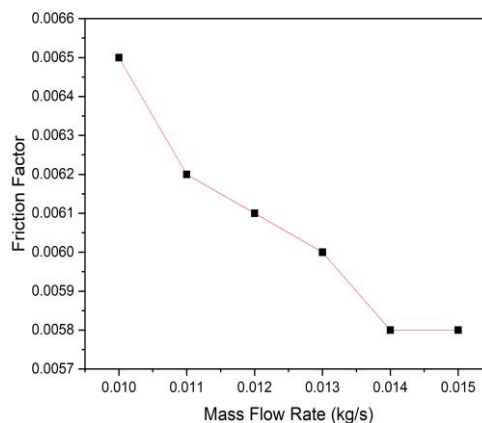


**Fig. 13:** Friction factor variation with mass flow rate

The experimental results reveal the variation of outlet and inlet air temperatures, as well as solar flux, throughout the day. Solar flux varied from 332 W/m<sup>2</sup> to 846 W/m<sup>2</sup> between 09:00 AM and 05:00 PM, with the peak solar flux observed between 12:00 PM and 01:00 PM. Experimental result of the designed triangular fined SAH shows, the maximum outlet temperature of the flowing air, which was achieved to be 59 °C at MFR of 0.010 kg/s and solar flux was 846 W/m<sup>2</sup>. Maximum rise in temperature of inlet air was achieved to be 24 °C around 12:00 PM. The maximum air temperature of 59 °C was reached at the lowest MFR of 0.010 kg/s, while the minimum outlet temperature of 57 °C occurred at the highest or peak MFR of 0.015 kg/s, around 12:00 PM. Temperature of the inlet air was increased by 56.66 % to 40.47 % along the time of day at the lowest MFR of 0.010 kg/s. Solar flux is varying from 436 W/m<sup>2</sup> - 846 W/m<sup>2</sup>; with the time of the day.

This study reveals that the pressure drops increase from 6 Pa to 18 Pa as the MFR ranges from 0.010 kg/s to 0.015 kg/s. Maximum pressure drop obtained at the highest MFR. The goal of minimizing pressure drop along the SAH duct was attained at the lower MFR of 0.010 kg/s. This study found a minimum variation of 6.25% in pressure drop (PD) between analytical and experimental results at a MFR of 0.010 kg/s, and a maximum variation of 30.55% at MFR of 0.015 kg/s. The variation in PD increased with higher MFR because of the presence of more fins.

This study reveals that the FF decreases as the Re increases. The FF drops from 0.0065 to 0.0058 as the MFR increases from 0.010 to 0.015 kg/s. At lower Reynold's numbers, the flow is laminar, leading to higher values of FF. As the Reynold's number increases, the flow transitions to turbulence, where inertial forces dominate, leading to a reduction in the friction factor.

#### Merits and Demerits of SAH

Solar air heaters (SAHs) have advantages over conventional heating systems due to their use of renewable energy technology, offering eco-friendliness,

low operating costs, and minimal maintenance. They effectively use solar energy for heating and crops drying, making them ideal for remote or off-grid areas. However, SAHs have some limitations, including reliance on sunlight, lower thermal efficiency, and limited heat output. They are less effective in cloudy conditions or at night operation, and some designs are bulky, requiring large surface areas for adequate energy collection.

#### Future research scope

Future research on SAHs should aim to boost thermal efficiency and cost-effectiveness by developing advanced materials for absorber plate, advance storage material, innovative absorber designs, and improved airflow mechanisms. Promising areas include integration with thermal storage, hybrid systems with photovoltaics, hybrid solar system combining panel cooling and air heating, and the use of automation and machine learning for real-time monitoring and performance optimization across varying climates. Efficient and cost-effective design can be developed also by using some optimization techniques like Rao algorithm, Response Surface Methodology (RSM), Taguchi, and Genetic algorithm (GA).

### Acknowledgments

This work was supported by the Mechanical Engineering Workshop, IFTM University, Moradabad, India for the fabrication of experimental setup.

### Nomenclature

$A_p$	Surface area of collector or absorber plate exposed to solar radiation ( $m^2$ )
$A_f$	Fluid flow area ( $m^2$ )
$A_c$	Surface area of glass cover plate ( $m^2$ )
$T_f$	Mean fluid temperature (K)
$T_{fi}$	Inlet temperature of flowing fluid or $T_i$ (K)
$T_{fo}$	Outlet temperature of flowing fluid or air (K)
$T_{air}$	Temperature of atmospheric air (K)
$T_c$	Temperature of toughened glass cover plate (K)
$T_p$	Mean temperature of collector or absorber plate (K)
$C_{pf}$	Specific heat of air (J/kgK)
$I$	Incident solar radiation or Solar flux ( $W/m^2$ )
$h_{cf}$	Heat transfer coefficient between cover plate and flowing fluid ( $W/m^2 K$ )
$h_{pf}$	Heat transfer coefficient between absorber plate and flowing fluid ( $W/m^2 K$ )
$U_{tl}$	Top heat loss coefficient ( $W/m^2 K$ )
$U_{bl}$	Bottom heat loss coefficient ( $W/m^2 K$ )
$U_{el}$	Edge heat loss coefficient ( $W/m^2 K$ )
$U$	Total heat loss coefficient ( $W/m^2 K$ )

$f$	Friction factor
$Pr$	Prandtl number
$F_R$	Collector heat removal factor
$Re$	Reynold's number
$Nu$	Nusselt number
$\dot{Q}_u$	Useful heat gain ( $W/m^2$ )
$\dot{Q}_c$	Incident solar flux ( $W/m^2$ )
$\dot{m}_f$	Mass flow rate of air (kg/s)
$D_h$	Hydraulic diameter (m)
$K$	Thermal conductivity of fluid (air)
$Pa$	Pascal ( $N/m^2$ )
Abbreviations	
SAC	Solar air collector
PD	Pressure drop
FF	Friction factor
SAH	Solar air heater
AP	Absorber plate
THP	Thermo-hydraulic performance
ASHRAE	American Society of Heating, Refrigerating and Air-Conditioning Engineers
Al	Aluminium
HTC	Heat transfer coefficient
TIG	Tungsten Inert Gas
MFR	Mass flow rate

#### Greek symbols

$\alpha$	Absorptivity of Al absorber plate or collector
$\epsilon_p$	Emissivity of Al absorber plate or SAC
$\epsilon_c$	Emissivity of toughened glazing
$\rho_{air}$	Density of flowing fluid ( $kg/m^3$ )
$\sigma$	Stefan-Boltz's man constant
$\mu_{air}$	Dynamic viscosity of flowing fluid ( $N\cdot s/m^2$ )
$\tau$	Solar transmittance of glazing
$\eta_{th}$	Thermal efficiency
$\Delta P$	Pressure drop

### References

- 1) E. Adi Saputro, E. Java Saputro, E. Java Bayu Wisnu Saputro, E. Java, W. Saputro, and B. Wisnu Saputro, "An investigation of engine performance and exhaust gas emissions under load variations using biodiesel fuel from waste cooking oil and b30 blend," *EVERGREEN Joint Journal of Novel Carbon Resource Sciences & Green Asia Strategy*, **10** (4) 2255–2264 (2023). doi:10.5109/7160901.
- 2) M. Filonchyk, M.P. Peterson, L. Zhang, V. Hurynovich, and Y. He, "Greenhouse gases emissions and global climate change: examining the influence of  $CO_2$ ,  $CH_4$ , and  $N_2O$ ," *Science of The Total Environment*, **935** 173359 (2024). doi:10.1016/J.SCITOTENV.2024.173359.
- 3) M. Kabir, U.E. Habiba, W. Khan, A. Shah, S. Rahim, P.R.D. los Rios-Escalante, Z.U.R. Farooqi, and L. Ali, "Climate change due to increasing concentration of carbon dioxide and its impacts on environment in 21st century; a mini review," *J King Saud Univ Sci*, **35** (5) 102693 (2023). doi:10.1016/J.JKSUS.2023.102693.

- 4) Syafrudin, M.A. Budihardjo, N. Yuliasuti, and B.S. Ramadan, "Assessment of greenhouse gases emission from integrated solid waste management in semarang city, central java, indonesia," *EVERGREEN Joint Journal of Novel Carbon Resource Sciences & Green Asia Strategy*, **8** (1) 23–35 (2021). doi:10.5109/4372257.
- 5) N.W. Arnell, S. Brown, S.N. Gosling, P. Gottschalk, J. Hinkel, C. Huntingford, B. Lloyd-Hughes, J.A. Lowe, R.J. Nicholls, T.J. Osborn, T.M. Osborne, G.A. Rose, P. Smith, T.R. Wheeler, and P. Zelazowski, "The impacts of climate change across the globe: a multi-sectoral assessment," *Clim Change*, **134** (3) 457–474 (2016). doi:10.1007/S10584-014-1281-2.
- 6) M.K. Barai, and B.B. Saha, "Energy security and sustainability in japan," *EVERGREEN Joint Journal of Novel Carbon Resource Sciences & Green Asia Strategy*, **2** (1) 49–56 (2015). doi:10.5109/1500427.
- 7) M. Indra al Irsyad, A. Soemanto, E. Mohi, and Y. Gunawan, "The role of oil fuels on the energy transition toward net zero emissions in indonesia: a policy review mohi, ervan planning bureau, ministry of energy and mineral resources the role of oil fuels on the energy transition toward net zero emissions in indonesia: a policy review," *EVERGREEN Joint Journal of Novel Carbon Resource Sciences & Green Asia Strategy*, **10** (4) 2074–2083 (2023). doi:10.5109/7160867.
- 8) Nurkamelia, Sugihardjo, B. Widarsono, Usman, Suliantara, S. Kepies, D. Dwiyanarti, D. Sunarjanto, M. Romli, and T.M. Susantoro, "Potential of ccs in east kalimantan's coal-power sector for achieving net-zero emissions," *EVERGREEN Joint Journal of Novel Carbon Resource Sciences & Green Asia Strategy*, **11** (3) 2555–2566 (2024). doi:10.5109/7236896.
- 9) A. Dwijatmiko, A. Nurrohim, J. Santosa, A. Sugiyono, A.H. Kuncoro, I. Rahardjo, A. Subandriya, and E. Siregar, "Optimizing electricity supply for jawa-madura-bali: scenarios for achieving net zero emissions," *EVERGREEN Joint Journal of Novel Carbon Resource Sciences & Green Asia Strategy*, **11** (3) 2567–2579 (2024). doi:10.5109/7236897.
- 10) S. Sharma, and R. Maithani, "A computational study on thermal and sustainability analysis of solar air heater with s and airfoil tabulators," *EVERGREEN Joint Journal of Novel Carbon Resource Sciences & Green Asia Strategy*, **11** (1) 295–305 (2024). doi: 10.5109/7172283.
- 11) S. Sharma, R. Maithani, and R.K. Das, "CFD based performance evaluation of solar air heater by using centerline perforated sine wave baffles," *EVERGREEN Joint Journal of Novel Carbon Resource Sciences & Green Asia Strategy*, **11** (2) 862–871 (2024). doi:10.5109/7183368.
- 12) S. Zaphar, M. Chandrashekara, and G. Verma, "Thermal analysis of an evacuated tube solar collector using a one-end stainless steel manifold for air heating applications under diverse operational conditions," *EVERGREEN Joint Journal of Novel Carbon Resource Sciences & Green Asia Strategy*, **10** (2) 897–911 (2023). doi:10.5109/6792885.
- 13) E.K. Akpınar, and F. Koçyiğit, "Experimental investigation of thermal performance of solar air heater having different obstacles on absorber plates," *International Communications in Heat and Mass Transfer*, **37** (4) 416–421 (2010). doi:10.1016/j.icheatmasstransfer.2009.11.007.
- 14) B.S. Romdhane, "The air solar collectors: comparative study, introduction of baffles to favor the heat transfer," *Solar Energy*, **81** (1) 139–149 (2007). doi:10.1016/J.SOLENER.2006.05.002.
- 15) B.F. Parker, M.R. Lindley, D.G. Colliver, and W.E. Murphy, "Thermal performance of three solar air heaters," *Solar Energy*, **51** (6) 467–479 (1993). doi:10.1016/0038-092X(93)90132-8.
- 16) D. Jin, S. Quan, J. Zuo, and S. Xu, "Numerical investigation of heat transfer enhancement in a solar air heater roughened by multiple v-shaped ribs," *Renew Energy*, **134** 78–88 (2019). doi:10.1016/J.RENENE.2018.11.016.
- 17) L.A. Rasheed, J.A.K. Mohammed, and R.A. Jessam, "Performance enhancement of solar air heater by integrating innovative absorber design and automatic control flow rate," *EVERGREEN Joint Journal of Novel Carbon Resource Sciences & Green Asia Strategy*, **10** (3) 1439–1448 (2023). doi:10.5109/7151693.
- 18) V.S. Hans, R.S. Gill, and S. Singh, "Heat transfer and friction factor correlations for a solar air heater duct roughened artificially with broken arc ribs," *Exp Therm Fluid Sci*, **80** 77–89 (2017). doi:10.1016/J.EXPTHERMFLUSCI.2016.07.022.
- 19) Varun, A. Patnaik, R.P. Saini, S.K. Singal, and Siddhartha, "Performance prediction of solar air heater having roughened duct provided with transverse and inclined ribs as artificial roughness," *Renew Energy*, **34** (12) 2914–2922 (2009). doi:10.1016/j.renene.2009.04.030.
- 20) R.S. Gill, V.S. Hans, J.S. Saini, and S. Singh, "Investigation on performance enhancement due to staggered piece in a broken arc rib roughened solar air heater duct," *Renew Energy*, **104** 148–162 (2017). doi:10.1016/J.RENENE.2016.12.002.
- 21) S. Panda, and R. Kumar, "A review on effect of various artificial roughness on heat transfer enhancement in a channel flow," *Journal of Thermal Engineering*, **7** (5) 1267–1301 (2021). doi:10.18186/THERMAL.978149.
- 22) N.K. Pandey, V.K. Bajpai, and Varun, "Experimental investigation of heat transfer augmentation using multiple arcs with gap on absorber plate of solar air heater," *Solar Energy*, **134** 314–326 (2016). doi:10.1016/J.SOLENER.2016.05.007.
- 23) K.S. Ong, "Thermal performance of solar air heaters:

- mathematical model and solution procedure,” *Solar Energy*, **55** (2) 93–109 (1995). doi:10.1016/0038-092X(95)00021-I.
- 24) K.S. Ong, “Thermal performance of solar air heaters—experimental correlation,” *Solar Energy*, **55** (3) 209–220 (1995). doi:10.1016/0038-092X(95)00027-O.
  - 25) K. Sopian, M.A. Alghoul, E.M. Alfegi, M.Y. Sulaiman, and E.A. Musa, “Evaluation of thermal efficiency of double-pass solar collector with porous–nonporous media,” *Renew Energy*, **34** (3) 640–645 (2009). doi:10.1016/J.RENENE.2008.05.027.
  - 26) D. Bahreghmand, and M. Ameri, “Energy and exergy analysis of different solar air collector systems with natural convection,” *Renew Energy*, **74** 357–368 (2015). doi:10.1016/J.RENENE.2014.08.028.
  - 27) H. Zhang, X. Ma, S. You, Y. Wang, X. Zheng, T. Ye, W. Zheng, and S. Wei, “Mathematical modeling and performance analysis of a solar air collector with slit-perforated corrugated plate,” *Solar Energy*, **167** 147–157 (2018). doi:10.1016/J.SOLENER.2018.04.003.
  - 28) Y. Khimsuriya, D.K. Patel, V. Patel, V. Pandit, H.S. Mohaisen, L.K. Kaushik, P. Mehta, and H. Patel, “Performance assessment of rotating spiral-shaped baffles built-in solar air heater: 4e and sustainability analysis,” *Case Studies in Thermal Engineering*, **72** 106345 (2025). doi:10.1016/J.CSITE.2025.106345.
  - 29) H.A. Maarof, M. Shamsi, M. Younas, and M. Rezakazemi, “Hybrid thermal and optical modeling of a solar air heater with a non-flat plate absorber,” *Energy Reports*, **9** 6102–6113 (2023). doi:10.1016/J.EGYR.2023.05.227.
  - 30) B.V. Kumar, C.P. Selvan, P.R. Kanna, D. Taler, M. Szymkiewicz, and J. Taler, “Numerical investigation of heat transfer enhancement in solar air heaters using polygonal-shaped ribs and grooves,” *Front Energy Res*, **11** 1279225 (2023). doi:10.3389/FENRG.2023.1279225/BIBTEX.
  - 31) Y.E. Bizuneh, T.D. Kassie, and A.E. Bizuneh, “Numerical studies on thermo-hydraulic performance of solar air heater with quarter circle roughness ribs,” *Scientific Reports 2025 15:1*, **15** (1) 1–11 (2025). doi:10.1038/s41598-025-10620-y.
  - 32) Y. Agrawal, J.L. Bhagoria, A. Gautam, A. Sharma, A.S. Yadav, T. Alam, R. Kumar, G. Goga, S. Chakroborty, and R. Kumar, “Investigation of thermal performance of a ribbed solar air heater for sustainable built environment,” *Sustainable Energy Technologies and Assessments*, **57** 103288 (2023). doi:10.1016/J.SETA.2023.103288.
  - 33) B.S. Romdhane, “The air solar collectors: comparative study, introduction of baffles to favor the heat transfer,” *Solar Energy*, **81** (1) 139–149 (2007). doi:10.1016/J.SOLENER.2006.05.002.
  - 34) A. Singh, V. Singh, V.R. Mishra, and V. Trivedi, “Optimizing the performance of the air-cooled microchip by the heat sink,” *Asia-Pacific Journal of Chemical Engineering*, e70114 (2025). doi:10.1002/APJ.70114.
  - 35) Niraj Kumar, M. K. Singh, V. S. Yadav, V. Singh, and A. Maheswari, “A comparative analysis of ribs and cans type solar air heater,” *EVERGREEN Joint Journal of Novel Carbon Resource Sciences & Green Asia Strategy*, **10** (3) 1449–1459 (2023). doi:10.5109/7151694.
  - 36) V. Singh, “Application of response surface methodology and computational fluid dynamics for analyzing and optimizing the performance of finned solar air heater,” *Proc Inst Mech Eng C J Mech Eng Sci*, **239** (1) 258–287 (2025). doi:10.1177/09544062241278187.
  - 37) D. Alta, E. Bilgili, C. Ertekin, and O. Yaldiz, “Experimental investigation of three different solar air heaters: energy and exergy analyses,” *Appl Energy*, **87** (10) 2953–2973 (2010). doi:10.1016/j.apenergy.2010.04.016.
  - 38) A.R. Jaurker, J.S. Saini, and B.K. Gandhi, “Heat transfer and friction characteristics of rectangular solar air heater duct using rib-grooved artificial roughness,” *Solar Energy*, **80** (8) 895–907 (2006). doi:10.1016/j.solener.2005.08.006.
  - 39) E.K. Akpınar, and F. Koçyiğit, “Energy and exergy analysis of a new flat-plate solar air heater having different obstacles on absorber plates,” *Appl Energy*, **87** (11) 3438–3450 (2010). doi:10.1016/j.apenergy.2010.05.017.
  - 40) B.M. Ramani, A. Gupta, and R. Kumar, “Performance of a double pass solar air collector,” *Solar Energy*, **84** (11) 1929–1937 (2010). doi:10.1016/j.solener.2010.07.007.
  - 41) H. Esen, “Experimental energy and exergy analysis of a double-flow solar air heater having different obstacles on absorber plates,” *Build Environ*, **43** (6) 1046–1054 (2008). doi:10.1016/j.buildenv.2007.02.016.
  - 42) A. Ucar, and M. Inalli, “Thermal and exergy analysis of solar air collectors with passive augmentation techniques,” *International Communications in Heat and Mass Transfer*, **33** (10) 1281–1290 (2006). doi:10.1016/j.icheatmasstransfer.2006.08.006.
  - 43) M. Akhbari, A. Rahimi, and M.S. Hatamipour, “Modeling and experimental study of a triangular channel solar air heater,” *Appl Therm Eng*, **170** 114902 (2020). doi:10.1016/J.APPLTHERMALENG.2020.114902.
  - 44) P.J. Bezbaruah, A. Das, R.S. Das, and B.K. Sarkar, “Numerical investigation on triangular fin-based solar air heater,” 341–350 (2020). doi:10.1007/978-981-15-2662-6\_31.
  - 45) W.H. Khalil, Z.A.H. Obaid, and H.K. Dawood, “Exergy analysis of single-flow solar air collectors with different configurations of absorber plates,” *Heat Transfer - Asian Research*, **48** (8) 3600–3616 (2019). doi:10.1002/HTJ.21558.
  - 46) M.H. Machi, M.A. Al-Neama, J. Buzás, and I. Farkas, “Energy-based performance analysis of a double pass

- solar air collector integrated to triangular shaped fins,” *International Journal of Energy and Environmental Engineering*, **13** (1) 219–229 (2022). doi:10.1007/S40095-021-00422-Z.
- 47) A.K. Albdour, Z.A.H. Obaid, M.S. Kamel, and I.D.J. Azzawi, “Energy, exergy, economic and environmental analysis of a solar air heater integrated with double triangular fins: experimental investigation,” *International Journal of Thermofluids*, **24** 100979 (2024). doi:10.1016/J.IJFT.2024.100979.
- 48) T.R. CJ, S. P, M. M M, and G. N, “Analytical investigation on thermo hydraulic performance augmentation of triangular duct solar air heater integrated with wavy fins,” *Int J Green Energy*, **20** (5) 544–554 (2023). doi:10.1080/15435075.2022.2111215.
- 49) P.I. Cooper, E.A. Christie, and R. V. Dunkle, “A method of measuring sky temperature,” *Solar Energy*, **26** (2) 153–159 (1981). doi:10.1016/0038-092X(81)90079-7.
- 50) W. Chang, Y. Wang, M. Li, X. Luo, Y. Ruan, Y. Hong, and S. Zhang, “The theoretical and experimental research on thermal performance of solar air collector with finned absorber,” *Energy Procedia*, **70** 13–22 (2015). doi:10.1016/J.EGYPRO.2015.02.092.
- 51) K. Sukhatme, and S.P. Sukhatme, “Solar Energy: Principles of Thermal Collection and Storage,” Tata McGraw-Hill, 1996. <https://books.google.co.in/books?id=1XHcwZo9XwC>.
- 52) J.A. Duffie, W.A. Beckman, and W.M. Worek, “Solar engineering of thermal processes, 2nd ed.,” *J Sol Energy Eng*, **116** (1) 67–68 (1994). doi:10.1115/1.2930068.
- 53) J.A. Duffie, and W.A. Beckman, “Selected heat transfer topics,” *Solar Engineering of Thermal Processes*, 138–172 (2013). doi:10.1002/9781118671603.CH3.
- 54) H.P. Garg, and J. Prakash, “Solar energy: fundamentals and applications,” Tata McGraw-Hill, 1997. <https://unesdoc.unesco.org/ark:/48223/pf0000150083> (accessed February 21, 2025).
- 55) H.K. Ghritlahre, P. Chandrakar, and A. Ahmad, “A comprehensive review on performance prediction of solar air heaters using artificial neural network,” *Annals of Data Science 2019 8:3*, **8** (3) 405–449 (2019). doi:10.1007/S40745-019-00236-1.
- 56) G.A. Hawkins, “Heat transmission . william h. mcadams. mcgraw-hill, new york-london, ed. 3, 1954. xiv + 532 pp. illus. \$8.50,” *Science* (1979), 120 (3128) 984–984 (1954). doi:10.1126/science.120.3128.984.a.
- 57) W.M. (William M. Kays, and (joint author.) Crawford M. E. (Michael E.), “Convective heat and mass transfer / w. m. kays, m. e. crawford,” (1980). [https://books.google.com/books/about/Convective\\_Heat\\_and\\_Mass\\_Transfer.html?id=PpkeAQAAIAAJ](https://books.google.com/books/about/Convective_Heat_and_Mass_Transfer.html?id=PpkeAQAAIAAJ) (accessed February 18, 2024).
- 58) S. Kumar, R.K. Das, and K. Kulkarni, “Comparative study of solar air heater (sah) roughened with transverse ribs of naca 0020 in forward and reverse direction,” *Case Studies in Thermal Engineering*, **34** 102015 (2022). doi:10.1016/J.CSITE.2022.102015.
- 59) R. Chandra, and M.S. Sodha, “Testing procedures for solar air heaters: a review,” *Energy Convers Manag*, **32** (1) 11–33 (1991). doi:10.1016/0196-8904(91)90139-A.
- 60) F. Incropera, D. DeWitt, T. Bergman, and A. Lavine, “Fundamentals of heat and mass transfer,” 1996. [http://www.mid-contracting.com/sites/default/files/webform/careers\\_webform/\\_sid\\_/pdf-fundamentals-of-heat-and-mass-transfer-frank-p-incropera-david-p-dewitt-pdf-download-free-book-7841c05.pdf](http://www.mid-contracting.com/sites/default/files/webform/careers_webform/_sid_/pdf-fundamentals-of-heat-and-mass-transfer-frank-p-incropera-david-p-dewitt-pdf-download-free-book-7841c05.pdf) (accessed February 22, 2025).
- 61) M. Assaye, M. Biadagegn, and B. Fekadu, “Numerical investigation of convection heat transfer in solar air heater with semi-circular shape transverse rib,” *Cogent Eng*, **9** (1) (2022). doi:10.1080/23311916.2022.2106930.
- 62) V. Singh, V.S. Yadav, A.B. Barnawi, J. Khan Bhutto, R. Verma, P. Singh, and N. Kumar, “Comparison of different designs of solar air heater with the simple solar heater of having reflecting mirrors,” *Proc Inst Mech Eng C J Mech Eng Sci*, **237** (21) 5156–5173 (2023). doi:10.1177/09544062231158530.
- 63) Vaibhav Trivedi, V. Singh, “A comprehensive review on development of solar pump operated by PV module,” *EVERGREEN Joint Journal of Novel Carbon Resource Sciences & Green Asia Strategy*, **11** (3) 1964–1989 (2024). doi.org/10.5109/7236845.
- 64) P.K. CHANG, “Thermal effects on separation of flow,” *Separation of Flow*, 608–715 (1970). doi:10.1016/B978-0-08-013441-3.50015-0.
- 65) S.Y. Ahn, and K.Y. Kim, “Thermal performance of t-shaped obstacles in a solar air heater,” *Processes 2020, Vol. 8, Page 1305*, **8** (10) 1305 (2020). doi:10.3390/PR8101305.
- 66) Varun, R.P. Saini, and S.K. Singal, “A review on roughness geometry used in solar air heaters,” *Solar Energy*, **81** (11) 1340–1350 (2007). doi:10.1016/J.SOLENER.2007.01.017.
- 67) S. Sharma, and R. Maithani, “A computational study on thermal and sustainability analysis of solar air heater with s and airfoil tabulators,” *EVERGREEN Joint Journal of Novel Carbon Resource Sciences & Green Asia Strategy*, **11** (1) 295–305 (2024). doi:10.5109/7172283.
- 68) N. Kumar, M.K. Singh, V.S. Yadav, V. Singh, and A. Maheswari, “An experimental investigation of ribbed solar air heater—free convection,” *Lecture Notes in Mechanical Engineering*, 373–381 (2022). doi:10.1007/978-981-16-5281-3\_35.
- 69) L.A. Rasheed, J.A.K. Mohammed, and R.A. Jessam,

- “Performance enhancement of a single pass solar air heater by adopting wire mesh absorber layer,” *EVERGREEN Joint Journal of Novel Carbon Resource Sciences & Green Asia Strategy*, **10** (2) 880–887 (2023). doi:10.5109/6792883.
- 70) G.K. Chhapparwal, A. Srivastava, and R. Dayal, “Artificial repeated-rib roughness in a solar air heater – a review,” *Solar Energy*, **194** 329–359 (2019). doi:10.1016/J.SOLENER.2019.10.011.
- 71) R. Kumar, V. Goel, P. Singh, A. Saxena, A.S. Kashyap, and A. Rai, “Performance evaluation and optimization of solar assisted air heater with discrete multiple arc shaped ribs,” *J Energy Storage*, **26** 100978 (2019). doi:10.1016/J.EST.2019.100978.
- 72) S. Zaphar, D.K. Saini, C. Muniyappa, and G. Verma, “Experimental investigation of enclosed steel tube fitted inside evacuated tube solar water heater using glazed aluminum reflector in two-stage heating,” *J Therm Anal Calorim*, **150** (14) 11127–11142 (2025). doi:10.1007/S10973-025-14426-Y/METRICS.
- 73) S. Zaphar, and G. Verma, “Enhancing the thermal efficiency and optimum temperature of a modified evacuated tube solar air collector by using the reflector,” *EVERGREEN Joint Journal of Novel Carbon Resource Sciences & Green Asia Strategy*, **10** (4) 2265–2276 (2023). doi:10.5109/7160902.
- 74) N. Madhwesh, K.V. Karanth, and S. Kumar, “Heat transfer enhancement of a solar air heater using capsule-shaped turbulators: a numerical analysis,” *Sci Rep*, **15** (1) 1–26 (2025). doi:10.1038/S41598-025-99294-0.
- 75) A. Kumar, R. Kumar, and A. Bhushan, “Differential exergy investigation and environ-economic assessment of a dimpled plate and flat plate solar air heater under turbulent conditions,” *Appl Therm Eng*, **240** 122299 (2024). doi:10.1016/J.APPLTHERMALENG.2023.122299.
- 76) M. Daadoua, B. Mathew, and F. Alnaimat, “Experimental investigation of pressure drop and heat transfer in minichannel with smooth and pin fin surfaces,” *International Journal of Thermofluids*, **21** 100542 (2024). doi:10.1016/J.IJFT.2023.100542.
- 77) A. Singh Yadav, and J.L. Bhagoria, “ICGSEE-2013 [14th-16th march 2013] international conference on global scenario in environment and energy a cfd analysis of a solar air heater having triangular rib roughness on the absorber plate,” *International Journal of ChemTech Research CODEN*, **5** (2) 964–971 (n.d.).
- 78) D. Wang, J. Liu, Y. Liu, Y. Wang, B. Li, and J. Liu, “Evaluation of the performance of an improved solar air heater with ‘s’ shaped ribs with gap,” *Solar Energy*, **195** 89–101 (2020). doi:10.1016/J.SOLENER.2019.11.034.
- 79) N.J. Yusaidi, M.F. Fauzan, A.F. Abdullah, A. Ibrahim, and A.A. Ishak, “Theoretical and experimental investigations on the effect of double pass solar air heater with staggered-diamond shaped fins arrangement,” *Case Studies in Thermal Engineering*, **60** 104619 (2024). doi:10.1016/J.CSITE.2024.104619.
- 80) V. Singh, and V.S. Yadav, “Optimizing the performance of solar panel cooling apparatus by application of response surface methodology,” *Proc Inst Mech Eng C J Mech Eng Sci*, **236** (22) 11094–11120 (2022). doi:10.1177/09544062221101828.
- 81) M. Daadoua, B. Mathew, and F. Alnaimat, “Experimental investigation of pressure drop and heat transfer in minichannel with smooth and pin fin surfaces,” *International Journal of Thermofluids*, **21** 100542 (2024). doi:10.1016/J.IJFT.2023.100542.
- 82) A. Kumar, A. Kumar, and G. Prasad, “Thermal and pressure drop analysis of solar air heater with and without wavy fin,” *International Journal of Mechanical Engineering and Technology (IJMET)*, **9** (12) 525–531 (2018). <http://iaeme.com/Home/issue/IJMET?Volume=9&Issue=12> (accessed March 3, 2025).
- 83) N.J. Yusaidi, M.F. Fauzan, A.F. Abdullah, and A. Ibrahim, “Numerical simulation of arrangement of diamond shaped fins in double pass solar air heater for drying application,” *2024 2nd International Conference on Power and Renewable Energy Engineering, PREE 2024*, 1–4 (2024). doi:10.1109/PREE63126.2024.10955836.
- 84) W. Ben Amara, A. Bouabidi, M. Chrigui, and E. Cuce, “A comparative study of helical and spiral flow paths in solar air heaters: experimental testing and cfd modeling,” *Renew Energy*, **244** 122642 (2025). doi:10.1016/J.RENENE.2025.122642.
- 85) H. Abulkhair, A.O. Alsaiani, I. Ahmed, E. Almatrafi, N. Madhukeshwara, and B.R. Sreenivasa, “Heat transfer and air flow friction in solar air heaters: a comprehensive computational and experimental investigation with wire-roughened absorber plate,” *Case Studies in Thermal Engineering*, **48** 103148 (2023). doi:10.1016/J.CSITE.2023.103148.
- 86) D. Singh, and V. Kumar, “Optimization of nusselt number and friction factor for a two-sided curvilinear rib-roughened solar air heater,” *Energy Sources, Part A: Recovery, Utilization, and Environmental Effects*, **47** (1) 5695–5713 (2025). doi:10.1080/15567036.2025.2467354.
- 87) G.R.K. Sastry, L.B.B. Raju, S.K. Gugulothu, Ü. Ağbulut, and P. Barmavatu, “Thermo-hydraulic optimization of rectangular duct solar air heaters using equilateral triangular roughness on absorber plates,” *J Therm Anal Calorim*, 1–19 (2025). doi:10.1007/S10973-025-14022-0/FIGURES/16.
- 88) A.O. Alsaiani, A. Iqbal, H. Abulkhair, L. Gzara, E. Almatrafi, H.A.H. Alzahrani, N. Madhukeshwara, B.M. Prasanna, and M. Aljohani, “Heat transmission and air flow friction in a solar air heater with a ribbed absorber plate: a computational study,” *Case Studies in Thermal Engineering*, **40** 102517 (2022). doi:10.1016/J.CSITE.2022.102517.

- 89) J. Blanco-Rodríguez, X. Simón-Montero, M. Cortada-García, S. Maroto, and P. Jacobo, "Modelling the impact of reducing lubricant viscosity on a conventional passenger car fuel economy and wear protection," *Results in Engineering*, **24** 103159 (2024). doi:10.1016/J.RINENG.2024.103159.